Lab on a Chip

Cite this: *Lab Chip*, 2011, **11**, 1671

www.rsc.org/loc

PAPER

Microchannels filled with diverse micro- and nanostructures fabricated by glancing angle deposition†

Louis W. Bezuidenhout,[a] Neda Nazemifard,[b] Abebaw B. Jemere,[c] D. Jed Harrison[bc] and Michael J. Brett*[ac]

Received 23rd December 2010, Accepted 9th March 2011
DOI: 10.1039/c0lc00721h

The integration of porous structures into microchannels is known to enable unique and useful separations both in electrophoresis and chromatography. Etched pillars and other nanostructures have received considerable interest in recent years as a platform for creating microchannels with pores tailored to specific applications. We present a versatile method for integration of three-dimensionally sculptured nano- and micro-structures into PDMS microchannels. Glancing angle deposition was used to fabricate nanostructures that were subsequently embedded in PDMS microchannels using a sacrificial resist process. With this technique, an assortment of structures made from a wide selection of materials can be integrated in PDMS microchannels; some examples of this versatility, including chiral and chevron nanostructures, are demonstrated. We also present a working device made using this process, separating 6/10/20 kbp and 10/48 kbp DNA mixtures in a DNA fractionator containing GLAD-deposited SiO_2 vertical posts as the separating medium. The separation mechanism was verified to resemble that found in prior fractionation devices, using total internal reflection fluorescence microscopy. GLAD fabrication enables insertion of three-dimensional structures into microchannels that cannot be fabricated with any existing techniques, and this versatility in structural design could facilitate new developments in on-chip separations.

1 Introduction

Microfluidic system capabilities and applications have grown rapidly over the past two decades.[1–4] Porous structure integration into microchannels has enhanced existing and introduced new microfluidic applications, particularly in electrophoretic and chromatographic separations.[5–8] Several different techniques have been developed for creating such porous channels, including micro- and nanofabricated pillars, solid particle packings, and porous monolith polymerization.[5–7] Direct fabrication of porous structures permits control of pillar/pore distributions, sizes, arrangements, homogeneity and architectures. This has led to faster and higher resolution separations[9] and has also provided access to unique separation mechanisms.[10–13]

Design and fabrication of separating media permits unique separation methods not achievable with traditional media. Creating pores smaller than a polymer's radius of gyration forces deformation at an entropic cost; this has been used to separate DNA by entropic recoil[14,15] and entropic trapping[16] in nanopillar arrays. The diffusional and thermodynamic characteristics of DNA and other molecules are exploited in separations on carefully designed "laterally asymmetric diffusion arrays", also known as Brownian ratchets,[13,17–19] and in separations by deterministic lateral displacement.[13,20] Two different configurations of sub-micron pillars have been used to demonstrate separation of the same DNA mixture by either size exclusion chromatography or electrophoresis.[21]

Volkmuth and Austin first used microfabricated pillars to create an artificial agarose gel with controllable porosity for studying electrophoretic DNA migration through porous matrices.[22] Several groups have subsequently separated DNA under constant and pulsed field electrophoresis in microchannel devices with microfabricated artificial sieves.[17,23–28] Nanofabricated pillars and porous alumina have been used to separate DNA *via* electrophoresis-driven size exclusion chromatography.[29,30] Artificial packed bed structures were fabricated for pressure-driven and electro-chromatographic separations of peptides and pigments.[9,31–35] Micro and nanofabricated porous structures have also been applied to microreactors,[36] catalysis beds,[37] DNA concentrators,[38] and an integrated microreactor and electrospray ionization tip.[39]

Our group previously reported the integration of microstructures fabricated using glancing angle deposition (GLAD) into microchannels.[40,41] Porous films of high aspect ratio sub-micron diameter sized structures can be deposited in a single step using

[a]*Department of Electrical and Computer Engineering, University of Alberta, T6G 2V4 Edmonton, Canada. E-mail: mbrett@ualberta.ca; Fax: +1-780-492-1811; Tel: +1-780-492-4438*
[b]*Department of Chemistry, University of Alberta, T6G 2G2 Edmonton, Canada*
[c]*National Institute for Nanotechnology, 11421 Saskatchewan Drive, T6G 2M9 Edmonton, Canada*

† Electronic supplementary information (ESI) available: Additional figures. See DOI: 10.1039/c0lc00721h

this physical vapor deposition approach. These structures are not limited to pillars, but can be sculpted into many different architectures during film fabrication.[42] Structures up to 10 μm tall are routinely deposited but can be taller. Heights are typically limited by deposition time, and by changes in film porosity that occurs as the height increases, leading to application-dependent height limits.

The integration of GLAD films in microfluidic systems is attractive for a number of reasons: precisely controlled morphology, compatibility with multiple materials, and demonstrated application to many systems. Films can have very high surface areas[43] and both the porosity and architecture can be finely controlled in three dimensions, *e.g.* porosity and structure can be varied in the plane of the device as well as through the thickness of the film (and consequently through the depth of the channel).[44] Many materials can be used, including insulators (*e.g.* SiO_2, Al_2O_3, TiO_2), semiconductors (*e.g.* Si, Ge) and metals (*e.g.* Ti, Zn, Cu); furthermore, heterostructures that combine different materials can also be grown.[45] GLAD films have been applied to applications that could benefit from integration with microfluidic systems, such as sensing,[46–48] thin layer chromatography,[49] and matrix-free laser desorption ionization.[50]

We have developed a flexible sacrificial etching technique that can be used to integrate GLAD-grown films into PDMS microfluidic channels with little limitation on film material and no limitation on film structure. Sacrificial etching techniques have previously been used to integrate micron and sub-micron sized fabricated pillar arrays into microchannels.[15,37,51–53] The versatility of this technique is demonstrated by filling channels with structures of different materials and architectures. Demonstrating the applicability of our process, we have performed DNA separation by fractionation in a pulsed electric field, using devices filled with SiO_2 GLAD porous films.

2 Materials and methods

2.1 Chemicals and materials

Films were deposited onto Corning 0211 glass substrates (10 cm × 10 cm, 0.5 mm thick, Corning Inc. Technical Materials, Corning, NY, USA) cut to appropriate sizes with a dicing saw, onto microscope cover glass (0.17 mm thick, Fisher Scientific Company, Ottawa, ON, CAN), or onto silicon wafers (Test Grade, 10 cm diameter, University Wafer, Boston, MA, USA). Evaporated materials, SiO_2 (>99.99% pure), Si (>99.999% pure), TiO_2 (>99.9% pure), Al_2O_3 (>99.99% pure) and Ag (>99.99% pure) were purchased from CERAC, Inc. (Milwaukee, WI, USA). Polydimethyl siloxane (PDMS) base and curing agent (Sylgard 184 silicone elastomer base and curing agent, Dow Corning Corporation, Midland, MI, USA) and the following chemicals were used during the fabrication process: HPR 506 and HPR 504 positive photoresist (Fujifilm Electronic Materials USA Inc., North Kingstown, RI, USA); AZ P4620 positive photoresist (AZ Electronic Materials USA Corp., Somerville, NJ, USA); Microposit 351 Developer (Shipley Company, L.L. C., Marlborough, MA, USA) diluted 1 : 4 on-site with deionized water; Microposit Remover 1165 (Shipley Company); methanol (>99.8% pure).

DNA samples, NoLimits™ DNA fragments (6 kbp, 10 kbp, 20 kbp, Fermentas Canada Inc., Burlington, ON, CAN) and λ-DNA (48 kbp, New England Biolabs Ltd., Pickering, ON, CAN) were stained by Molecular Probes YOYO-1 (Invitrogen Canada Inc., Burlington, ON, CAN) with a dye-to-base ratio of 1 : 10. Pulsed field electrophoresis was performed in 4 × TBE buffer (356 mM tris-borate, 8 mM ethylenediamine tetra-acetic acid, pH 8.3) to suppress electroosmotic flow, with 4% v/v 2-mercaptoethanol added to reduce photobleaching. The apparatus and experimental setup used for DNA fractionation have been described elsewhere.[54] For single DNA imaging, a motorized total internal reflection fluorescence microscopy (TIRF) system was used with a 60× oil-immersion objective (Nikon Canada Inc., Mississauga, ON, CAN). TIRF microscopy is specially designed to enable single molecule visualization with a high signal to noise ratio. Scanning electron micrographs were taken of devices during and after fabrication with an Hitachi S-4800 field emission scanning electron microscope.

2.2 Fabrication process

A sacrificial etch process was developed to fabricate microfluidic devices with GLAD structure-filled channels (Fig. 1). First, the GLAD nanostructures were deposited onto a clean, flat substrate. The porous film was filled with photoresist by spin application, and the resist was photolithographically patterned to define the microfluidic channels. The entire substrate was coated with PDMS, which was then cured. Fluid reservoirs that also served as access holes for the sacrificial etch were punched or cut out of the PDMS. A sacrificial etch was used to remove the photoresist from the microfluidic channels, and the device was

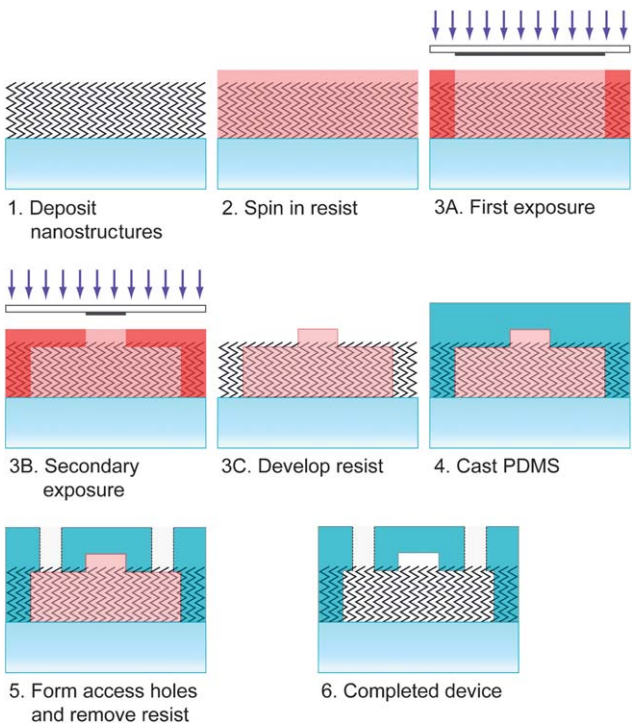

Fig. 1 Process used to fabricate microchannels with embedded GLAD-deposited micro- and nanostructures.

dried to complete the fabrication process. Each process step is described in detail as follows:

2.2.1 GLAD deposition. All substrates (glass or silicon) were cleaned prior to deposition using a Piranha etch (3 : 1 sulfuric acid and hydrogen peroxide) and air dried. GLAD films were deposited to the desired thickness by electron-beam evaporation of the target material (SiO_2, Si, TiO_2, Al_2O_3, or Ag) onto a substrate in a custom-made high-vacuum deposition system (AXXIS, Kurt J. Lesker Co., Clairton, PA), evacuated to a base pressure of 8×10^{-5} Pa or lower. Corning 0211 glass was used to make functional transparent devices amenable to laser induced fluorescence, thin microscope slide cover glasses were used to make devices for TIRF microscopy, and silicon was used to produce samples that could be easily cleaved for scanning electron microscopy imaging. Deposition rates as measured for a normal-oriented substrate by a quartz crystal microbalance varied between 1.2 nm s^{-1} and 2.0 nm s^{-1}; effective deposition rates are lower at oblique deposition angles. The films presented here ranged in thickness from 4 μm to 7 μm.

2.2.2 Photoresist application. HPR 506 was spun into films with a 500 rpm, 10 s spread phase followed by a 40 s spin phase with a rotation rate dependent on the film structure, film thickness, film porosity and the desired resist thickness. Typically, a rate between 1500 rpm and 2000 rpm was used for films 5 μm to 6 μm tall. The substrate and photoresist were baked for 90 s at 115 °C to remove residual solvent and were left to equilibrate to room humidity for more than 30 min. The resist completely infiltrates the GLAD film,[41,55] and an overburden of photoresist typically remains on top of the structures after spinning in the resist, shown schematically in Fig. 1.2.

2.2.3 Photoresist patterning. The desired microchannel pattern was transferred to the photoresist using standard photolithography techniques (chromium mask, 405/365 nm filtered mercury arc lamp). When needed, a second exposure was performed either without a mask, or through a second mask aligned to features defined by the first mask—these features were visible in the slight change in resist color following the first exposure. This second exposure was used to fine tune the height of the channels by altering the resist thickness through a combination of spin-in velocity and secondary exposure time. In this fashion structures could either be sealed to the ceiling of the device, or a space could be left between the tops of the structures and the device ceiling (both illustrated in Fig. 1.3). Exposed resist was etched away by agitation in developing solution for 35 s, followed by a deionized water rinse and drying with nitrogen.

2.2.4 PDMS application. PDMS was prepared by mixing the base and curing agent in a 10 : 1 ratio and degassing under house vacuum (~7 bar). The PDMS was then slowly poured onto the devices to the desired thickness, typically 1–3 mm thick. It was contained by clamping an aluminium ring and rubber gasket to a silicon wafer resting on an aluminium plate, with the devices taped down on the wafer. The PDMS penetrates into the exposed inter-pillar spaces and surrounds the photoresist-filled channels. Curing was accelerated by baking the assembly in an oven at 50 °C for four hours.

2.2.5 Sacrificial material removal. PDMS plugs were removed from the devices to create fluid reservoirs; plugs were either gently punched out using a metal punch pushed into the PDMS until it reached the top of the substrate, or were cut into the PDMS using a scalpel. These reservoirs also served as access ports for dissolution and removal of the sacrificial photoresist. The devices were soaked for 24 h in 1-methyl-2-pyrrolidone (Microposit Remover 1165) followed by a second 16 h soak in a fresh batch of 1165. A final 16 h soak in methanol was used to rinse any remaining resist and remover from the channels. The methanol was allowed to evaporate from the channels, and the devices were stored until use.

2.3 DNA separation

To perform a molecular separation, we fabricated DNA fractioners based on the design by Zeng *et al.*,[54] first described by Huang *et al.*,[12] replacing the self-assembled porous colloidal array with SiO_2 GLAD structures. A vertical post film was deposited by continuously rotating the substrate at a rate of one revolution per 50 nm of film growth, at a deposition angle of 85°. This film has a porosity of approximately 80%.[43] The posts were then encapsulated in PDMS channels using the procedure outlined above. A brief mask-less second exposure during lithography removed a thin layer of photoresist, exposing the tips of the posts; these tips were subsequently embedded in the PDMS channel ceiling, creating a seal that prevented fluid shunting between the ceiling and top of the posts.

The device fluid reservoirs were filled with 4 × TBE solution to reduce electroosmotic counterflow. The PDMS hydrophobicity prevented TBE from entering dry channels; this problem was circumvented by first wetting the channels with methanol, then replacing methanol in the fluid reservoirs with TBE solution. DNA mixture—6/10/20 kbp or 10/48 kbp—was added to the inlet reservoir.

The apparatus and separation protocol have been discussed in detail elsewhere.[54,56] Briefly, DNA is continuously injected into a square chamber containing a sieving matrix. An alternating asymmetric electric field applied across the separation chamber fractions the DNA into streams of different DNA sizes. The electric field changes its direction between one which is perpendicular to the DNA inlet (E_1) and the second one which is oriented 135° relative to the first one, with a vertical component pointing towards the DNA inlet (E_2) (see Fig. 5c). In all of our experiments $E_2 = 1.4E_1$. The electric field (E_1) was varied between 85 and 260 V cm^{-1}, while the frequency was varied between 0.1 and 20 Hz to obtain optimum separation resolution.

3 Results and discussion

Complete infiltration of photoresist into GLAD films is necessary for the sacrificial process presented here. Fig. 2 shows an SiO_2 vertical post GLAD film filled with HPR 506 photoresist before and after short UV exposures and subsequent development. The deposited structures are firmly embedded in the photoresist. The figure also demonstrates how short exposures can be used to controllably reveal the structure's top. The tips of the posts are increasingly exposed as the exposure time increases from 0.4 s to 1.2 s. Fig. S1† shows the resist overburden being

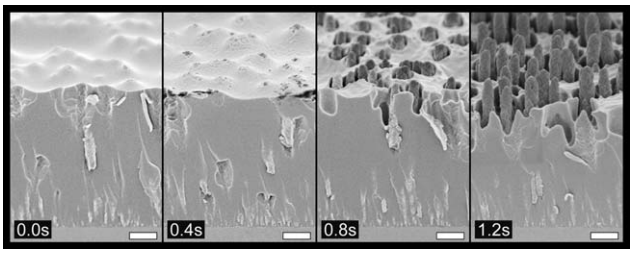

Fig. 2 Scanning electron micrographs showing how the amount of photoresist removed to reveal the underlying structures changes with UV exposure times (shown in seconds) for vertical posts grown at $\alpha = 88°$ with little overburden. Scale bar indicates 1 μm.

removed from a Si chevron film by exposure for 1.2 s through a chrome mask (with no exposure on the masked left side) and subsequent development of exposed resist.

The overburden thickness remaining on top of the structures after spinning in the resist depended on a number of film properties, including porosity (*i.e.* deposition angle), material, architecture, and height. For a given film, the overburden thickness depended on the spin speed and resist viscosity. The overburden was reduced with thicker and more porous (lower density) films, less viscous resists, or faster application speeds. The devices discussed in this report were fabricated using HPR 506 resist, which left a thin overburden on films approximately 5 μm high. Other resists such as HPR 504 (a less viscous resist) and AZ P4620 (a more viscous resist) have also been successfully used for this process. For the film thicknesses used here, the less viscous resist sometimes caused compressive deformation of the films, discussed below, or incompletely filled the film, while the more viscous resist formed an unnecessarily thick overburden.

As the spin-in speed was increased, the overburden thickness decreased, until a threshold speed was reached where almost no overburden remained. At this threshold, there is a transition from an overburden to a thin layer of photoresist that coats the top of the GLAD film, as can be seen in Fig. 2 at 0 s exposure time. Increasing the speed further did not reveal increasing amounts of film; instead, we observed film compression by the thinning photoresist layer at higher speeds.

The centrifugal forces did not noticeably alter the vertical orientation of the GLAD structures at low spin speeds, where an overburden remained; however, the film compression observed at speeds past the overburden threshold indicated that some deformation was likely present at higher speeds. Examination by scanning electron microscopy suggests that the source of this compression depended on film architecture, and was possibly due to deformation of the film by spring-like compression, tilting of the columns in the case of incompressible structures (*e.g.* vertical posts), or a combination of the two mechanisms.

Fig. 3 shows cross sectional scanning electron micrographs (SEMs) of fabricated channels before and after resist dissolution, revealing how both the photoresist and PDMS completely infiltrated the GLAD film, with a clear boundary forming between the two polymers. Resist removal was selective, leaving behind GLAD structures surrounded by PDMS walls. The structures in Fig. 3a are slightly embedded in the PDMS ceiling and no deformation or clumping of the film was observed other than a few posts dislodged by the SEM sample preparation process.

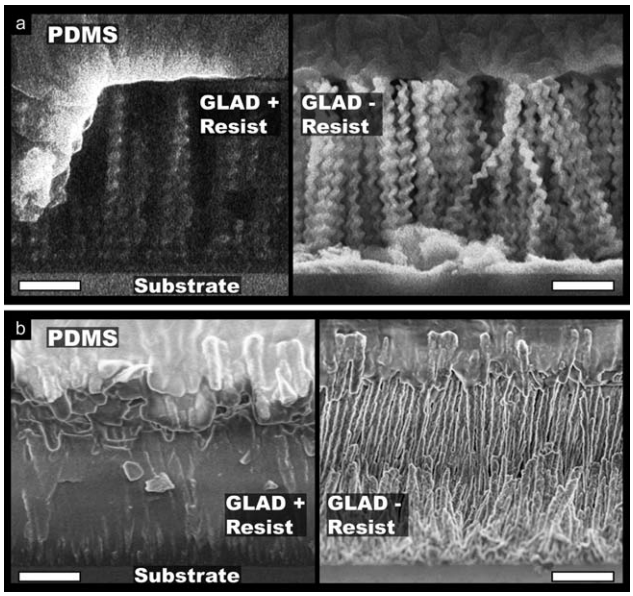

Fig. 3 A microchannel containing GLAD-deposited (a) SiO_2 hexagonal spirals ($\alpha = 84.5°$) and (b) SiO_2 micropillar vertical posts ($\alpha = 83.5°$) before (L) and after (R) removing the sacrificial photoresist. Scale bars indicate 2 μm.

The top ~1 μm of the vertical posts in Fig. 3b are firmly embedded in the PDMS. The posts in the foreground were fractured during the cleaving process with the top half removed along with the PDMS; these short posts subsequently clumped during the drying process. It is difficult to see the inter-pillar spaces in the exposed vertical post film due to the mixed-detection mode necessary to limit charging effects that can saturate the detector during SEM imaging of this sample; however, close inspection of the pillar surfaces revealed the roughened morphology characteristic of SiO_2 GLAD posts, confirming removal of the photoresist polymer from the channel.

Fig. 4 shows various GLAD structures embedded in PDMS microchannels, demonstrating the flexibility of the process in making arbitrary structures for embedding in microchannels. Vertical posts such as those shown in Fig. 2 and 3b are most similar to structures that can be made using other methods such as microfabrication, where a geometry is etched downwards into the substrate. Fig. 4a–e demonstrate how film architecture can be controlled during deposition to give various structures. Fig. 4f and 4g shows a trimaterial, triarchitectural structure, where silver slanted posts have been sandwiched between silicon dioxide hexagonal staircase spirals and aluminium oxide square spirals. Fig. 4f shows the emptied channel alongside the PDMS-filled film area that constitutes the channel wall. The film in Fig. 4g has been fractured at the Ag-SiO_2 interface during SEM sample preparation, with the square spirals embedded and retained in the elevated channel ceiling. It should be emphasized that in most cases, the material and structures are interchangeable – that is, the film shown in Fig. 4a could have been made with Si or TiO_2, and likewise the film in Fig. 4f could have been made with the same structure but a different combination of materials. As with Fig. 3a, the interpillar spaces are difficult to see in Fig. 4b, 4f and 4g due to the SEM detection mode used to limit charging effects.

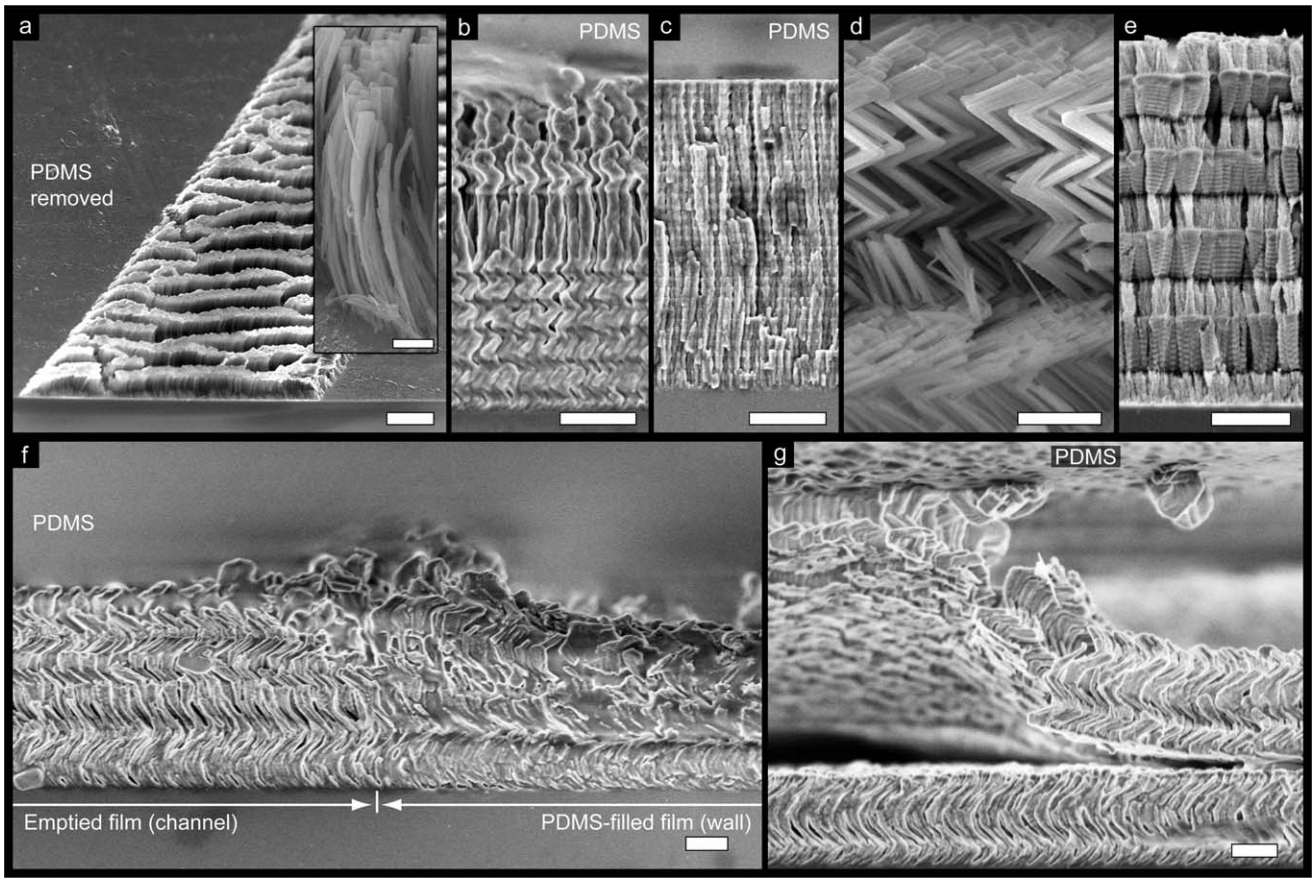

Fig. 4 Scanning electron micrographs of glancing angle deposition films embedded in PDMS microchannels, demonstrating structures that can be integrated in microchannels using GLAD: (a) SiO_2 'blades' where the surrounding PDMS has been torn away to reveal the anisotropic structures ($\alpha =$ 87°, inset shows magnified view of structures), (b) SiO_2 helix/vertical post/helix heterostructure ($\alpha = 84°$), (c) TiO_2 periodically graded density film (α oscillating between 60° and 80°), (d,e) Si chevrons ($\alpha = 85°$) with torn-away PDMS, and (f,g) SiO_2 hexagonal spiral/Ag slanted post/Al_2O_3 square spiral heterostructure ($\alpha = 85°$). Scale bars indicate 1 μm in (b)–(g) and (a, inset), and 10 μm in (a).

Fig. 4c illustrates how the porosity for a given film architecture can be adjusted by changing the substrate deposition angle. In this film, the deposition angle was periodically oscillated between 60° and 80°. As the deposition angle decreases, the intercolumn pores and column diameters become smaller. At the same time, the surface area increases to a maximum at a deposition angle of approximately 60°, depending on film material.[43] In this way, devices can be tuned for specific applications: very high surface areas may be more desirable for some microreactors, small pores formed at low deposition angles may be optimal for separating small molecules, whereas large pores formed at high deposition angles may be best for separating large DNA strands or proteins. A combination of high surface area and large pores can be obtained by altering the deposition angle throughout film growth as shown in Fig. 4c.

The structures in Fig. 4a, 4d and 4e have in-plane anisotropy built into the film structure during deposition. Vertical pores in between the blade-like structures in (a) extend through the height of the film, but one can see from this image that the width of these pores depend on the direction one takes across the substrate (and hence through the film), with maxima and minima orthogonal to each other. The PDMS layer has been peeled off prior to photoresist removal, resulting in clumping of the bladed nanostructures, shown in closer detail in the inset. The blades are oriented with their flat faces pointing in the direction of the channel (vertically), and clumping is preferential between these high surface area flat sides resulting in the formation of horizontal lines of clumped structures. This clumping and subsequent bi-modal porosity was not present in the fabricated channel prior to removal of the PDMS channel. The chevron structure in (d) and (e) has a more pronounced in-plane porosity difference, with narrow pores along one direction (e) and wide, almost channel-like pores in the perpendicular direction (d). This kind of lateral asymmetry in microfabricated devices has been shown to provide novel separation schemes; for example, Fu *et al.* fabricated two-dimensional devices with laterally asymmetric channel heights to create a 2-D array for separations with independent control over separation speed and resolution *via* either entropic trapping or Ogston sieving.[10]

Changes in the substrate orientation during deposition can alter the film structure dramatically. This provides control over the column architecture throughout the height of the channel, as seen in Fig. 4b and 4d–g. Porosity differences arising from altering the deposition angle during growth correspond with density changes in the film, which in turn alter the effective optical index of refraction. Periodically graded density optical

filters that transmit a pre-determined wavelength of light and porous optically responsive humidity sensors have been made using this effect.[42] Fig. 4c shows such a periodically graded density structure integrated into a microchannel, formed by continuously oscillating the deposition angle to produce alternating layers of high and low film density. In this way, porous optical elements that can potentially respond to changes in the penetrating fluid can be built directly into microchannels. While not shown here, these porosity changes can be combined with architectural changes such as those in Fig. 4b, 4d and 4g for an added dimension of structural control.

High aspect ratio micro- and nanostructures tend to clump or cluster together upon drying after immersion in liquids, possibly due to capillary forces acting on the structures as the fluid evaporates.[37,57] Post-deposition ion-milling of posts[58] or specialized drying procedures, such as freeze drying[37] or critical point drying, can be used to minimize or eliminate this phenomenon. This kind of clumping in GLAD films has been shown to be predictable and dependent on film architecture,[59] and thus may be exploited in some microfluidic applications where a bimodal micro/nano-porous pore distribution is desirable. The fabrication process presented here also provides another option for eliminating clumping when it is undesirable. When the tops of the columns are embedded in the PDMS ceiling (*e.g.* Fig. 3b), clumping is eliminated. Fixation at the top and bottom prevents capillary forces from pulling columns together during the drying process.

The tendency for PDMS to swell when immersed in solvents[60] has to be taken into consideration in this fabrication process. Swelling from certain solvents, *e.g.* isopropanol and acetone, was found to be severe enough to cause delamination of PDMS from the substrate surface for some of our devices. We found that neither 1-methyl-2-pyrrolidone nor methanol caused an appreciable amount of swelling, even after soaking PDMS over a number of days. Consequently 1-methyl-2-pyrrolidone was used instead of acetone to dissolve the sacrificial photoresist, and methanol was preferred for removing 1-methyl-2-pyrrolidone from the channels. As with any PDMS-based device, this has implications on the solvents suitable for regular use within the device. The process described here could be extended to a variety of materials in cases where the properties of PDMS are undesirable. GLAD films have been filled with other materials including polystyrene, metals (*e.g.* gold, nickel) and polymers (*e.g.* acrylates),[55,61] and these could replace PDMS in the fabrication process.

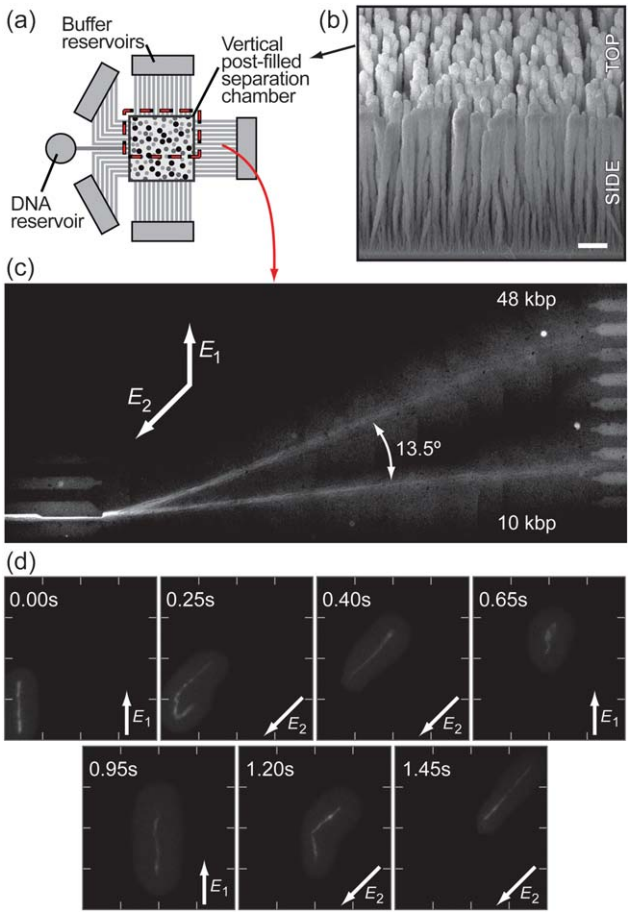

Fig. 5 (a) Schematic of the microfluidic chip fractionator used for separating DNA, filled with GLAD posts as a separation matrix. DNA mixture is injected from the reservoir into the separation chamber (left to right). Pulsed electric fields are applied across the chamber by platinum electrodes placed in the buffer reservoirs. (b) Scanning electron micrographs showing an oblique view of the vertical post nanostructured thin film used for separating DNA (Scale bar indicates 1 μm. Top and side views are shown in Fig. S2†). (c) Fluorescence image of the separation chamber. Two different sizes of DNA, 10 kbp and 48 kbp, are injected into the chamber from the left and separate to form two different streams moving towards the collection channels at the end of the separation chamber. Applied electric fields were $E_1 = 60$ V cm^{-1} and $E_2 = 84$ V cm^{-1} as indicated by the arrows, switched at frequency 2 Hz. Image was assembled from multiple 320 × 200 px screen captures. The two white dots are debris. (d) Time elapsed fluorescence images (TIRF microscopy) of 48 kbp DNA molecules migrating in the separation chamber, with applied electric fields of $E_1 = 80$ V cm^{-1} and $E_2 = 112$ V cm^{-1} as indicated by the arrows, at frequency 1 Hz.

3.1 DNA separation

We fabricated a fractionation device that confirmed GLAD posts could act as a porous matrix for DNA separation. Fig. 5b and Fig. S2† reveal the porous vertical post film used for this separation, prior to integration into microchannels. Such films have an inter-column spacing of approximately 115 nm on average.[62] Fig. 5a shows a schematic of the microfluidic device, where the separation chamber was filled with the GLAD posts shown in Fig. 5b as a sieving matrix. Using this device, a mixture of 10 kbp and 48 kbp DNA was separated into individual streams, as shown in Fig. 5c. These streams can be collected into different channels at the end of the separation chamber. Arrows indicate the direction and relative magnitude of the asymmetric electric fields applied across the chamber *via* the buffer reservoirs to effect the separation.

Separation resolution is dependent on the pulsed field frequency; on this particular device, an optimum separation of 13.5° between 10 kbp and 48 kbp DNA was obtained at a frequency of 2 Hz (see Fig. S3†). The optimum frequency depends on a number of factors, including the size range of the DNA being separated.[54,56] Using an identical device (same porous film and fabrication process), we were also able to

separate a mixture of 6, 10 and 20 kbp DNA into three streams at an optimum frequency of 15 Hz (data not shown). We performed separations on multiple devices. The yield of functional devices was 50%, with DNA separation data reproducible within a standard deviation of 10%.

TIRF microscopy was used to observe the migration mechanism of DNA molecules through the GLAD posts. Fig. 5d shows seven sequential fluorescence images extracted from a captured real time movie of an isolated 48 kbp DNA molecule moving under fields of $E_1 = 80$ V cm^{-1} and $E_2 = 112$ V cm^{-1} at a frequency of 1.0 Hz. As seen in these images, DNA molecules stretch and move in an opposite direction to the applied field, usually led by one of their ends. Once the direction of the electric field changes, the molecules are reoriented and backtrack away from the new direction, now led by the head that was previously the tail. Our observations show that the DNA migration mechanism under pulsed electric fields in GLAD post arrays is very similar to the migration mechanism of DNA molecules in nanoparticle arrays[54] and microfabricated post arrays.[12]

This separation demonstrates that an unmodified GLAD film is effective as a separation matrix. We observed a small amount of dispersion in these preliminary separations, evident by broadening of the DNA streams as they progress through the array to the collection channels. This dispersion was quantified by calculating the fluorescence intensity profile peak variance σ^2 of the 10 kbp stream shown in Fig. 5c.[63] Comparison of the variances at the injection point (σ_I^2) and at a point 2.6 mm downstream of the injection point (σ_T^2) allows for calculation of the band broadening caused by contributing factors (σ_F^2) other than the injection, where $\sigma_T^2 = \sigma_I^2 + \sigma_F^2$. Such factors can include DNA diffusion, DNA size fluctuations, electric field gradient, and structural defects or disorder in the separation matrix. For the vertical post GLAD fractionator shown here, $\sigma_F = 20$ μm ± 15%. This was the same as the dispersion (within error), $\sigma_F = 18$ μm ± 15%, on a similar device with a self-assembled nanosphere array matrix using the same size DNA and similar conditions[63] ($\sigma_T = 22$ μm for both devices), despite distinct physical differences between the two matrices. The nanosphere array has a comparable porosity to the GLAD film (700 nm diameter silica spheres forming approximately 100 nm sized pores), but a very low amount of disorder and inhomogeneity in pore size and distribution in contrast to the GLAD film's high surface area and unoptimized larger pore size distribution. The separation performance of our device was comparable to that of similar-sized DNA using devices based upon the same separation mechanism.[19,63]

The high surface areas present in nanopillar films can cause band broadening due to surface area dependent electroosmotic flow (EOF).[64] The mobility for 48 kbp DNA in our device was $\mu = 2.5 \times 10^{-5}$ cm^2 V^{-1} s^{-1} ± 15%, calculated using TIRF microscopy images ($E = 114$ V cm^{-1}). This is comparable to the nanosphere array device, with similar porosity and negligible EOF, where $\mu = 2.8 \times 10^{-5}$ cm^2 V^{-1} s^{-1} ± 15% ($E = 114$ V cm^{-1}).[63] Thus EOF was sufficiently suppressed by the buffer and is not expected to have played a role in band broadening.

Pore and column size inhomogeneity may cause dispersion during DNA fractionation.[63] As seen in Fig. 5b and Fig. S2†, there is a range of pore sizes present in GLAD films as a result of column extinction and broadening during growth.[43,65] The net effect is to create a pore gradient through the height of the film, with pore size increasing along the height of the film. This pore inhomogeneity is expected to have contributed to the observed dispersion in our device, and is likely also responsible for a significant portion of the background fluorescence observed during the separation—scattering of emitted light through the silica structures resulted in noticeable levels of background light.

Two strategies that have been shown to be effective in reducing this inhomogeneity within GLAD films could be used to optimize separations and minimize band-broadening dispersion: deposition onto pre-patterned substrates can create regularly spaced structures with very narrow and controllable pore size distributions;[66,67] post-deposition ion milling can smooth columns while removing the remnant extinguished posts that contribute to the film pore gradient.[58] Both processes are compatible with the fabrication process described here.

4 Conclusions

The increased surface area, controllable porous network structure, and varied morphologies of fabricated porous microchannels have found numerous uses in miniaturized systems. We have developed a fabrication method that provides a versatile technique for integrating micro- and nanostructures into microchannels, as demonstrated by the various architectures and materials that can be integrated in channels using glancing angle deposition. Engineered three-dimensional Si, SiO_2, TiO_2, Al_2O_3, and Ag structures were grown with GLAD and incorporated into PDMS microchannels using a sacrificial etch technique. Separation of DNA mixtures (sizes between 6 kbp and 48 kbp) into individual streams in a fractionation array verified that this technique could be used to fabricate working microfluidic devices. To our knowledge, this is the first report of such a technique for creating microfluidic channels containing nano- and microstructures with engineered, controllable three-dimensional architectures.

The separation presented here was one example of a working device fabricated with glancing angle deposition. Further work will investigate tuning of pore sizes to enable and optimize on-chip DNA and protein separations. This work also enables applications that can utilize the versatility afforded by pore size and shape engineering, and the ability to sculpt the structure morphology along the height of the film. Such structures are difficult to impossible to fabricate using competing techniques.

Acknowledgements

Support for this work was generously provided by the Natural Sciences and Engineering Research Council of Canada, the NRC-CNRC National Institute for Nanotechnology, Alberta Innovates – Technology Futures, and Micralyne Inc. The authors thank the University of Alberta for support of the NanoFab, and would also like to thank Mr Martin Kupsta and Mr Jaron van Dijken for SEM imaging, and Dr Michael T. Taschuk, Dr Anastasia Elias and Dr Eric Flaim for valuable discussions concerning this work.

References

1 A. van den Berg, H. G. Craighead and P. Yang, *Chem. Soc. Rev.*, 2010, **39**, 899–900.
2 K. Ohno, K. Tachikawa and A. Manz, *Electrophoresis*, 2008, **29**, 4443–4453.
3 J. West, M. Becker, S. Tombrink and A. Manz, *Anal. Chem.*, 2008, **80**, 4403–4419.
4 G. M. Whitesides, *Nature*, 2006, **442**, 368.
5 J. Fu, P. Mao and J. Han, *Trends Biotechnol.*, 2008, **26**, 311–320.
6 N. Kaji, Y. Okamoto, M. Tokeshi and Y. Baba, *Chem. Soc. Rev.*, 2010, **39**, 948–956.
7 M. De Pra, W. Th. Kok and P. J. Schoenmakers, *J. Chromatogr., A*, 2008, **1184**, 560–572.
8 J. C. T. Eijkel and A. van den Berg, *Electrophoresis*, 2006, **27**, 677–685.
9 M. De Pra, W. De Malsche, G. Desmet, P. J. Schoenmakers and W. Th. Kok, *J. Sep. Sci.*, 2007, **30**, 1453–1460.
10 J. Fu, R. B. Schoch, A. L. Stevens, S. R. Tannenbaum and J. Han, *Nat. Nanotechnol.*, 2007, **2**, 121–128.
11 M. Cabodi, Y.-F. Chen, S. W. P. Turner, H. G. Craighead and R. H. Austin, *Electrophoresis*, 2002, **23**, 3496–3503.
12 L. R. Huang, J. O. Tegenfeldt, J. J. Kraeft, J. C. Sturm, R. H. Austin and E. C. Cox, *Nat. Biotechnol.*, 2002, **20**, 1048–1051.
13 L. R. Huang, E. C. Cox, R. H. Austin and J. C. Sturm, *Science*, 2004, **304**, 987.
14 S. W. P. Turner, M. Cabodi and H. G. Craighead, *Phys. Rev. Lett.*, 2002, **88**, 128103.
15 M. Cabodi, S. W. P. Turner and H. G. Craighead, *Anal. Chem.*, 2002, **74**, 5169–5174.
16 J. Han and H. G. Craighead, *Science*, 2000, **288**, 1026.
17 T. A. J. Duke and R. H. Austin, *Phys. Rev. Lett.*, 1998, **80**, 1552–1555.
18 C. F. Chou, O. Bakajin, S. W. P. Turner, T. A. J. Duke, S. S. Chan, E. C. Cox, H. G. Craighead and R. H. Austin, *Proc. Natl. Acad. Sci. U. S. A.*, 1999, **96**, 13762.
19 L. R. Huang, E. C. Cox, R. H. Austin and J. C. Sturm, *Anal. Chem.*, 2003, **75**, 6963–6967.
20 D. W. Inglis, J. A. Davis, R. H. Austin and J. C. Sturm, *Lab Chip*, 2006, **6**, 655–658.
21 M. Baba, T. Sano, N. Iguchi, K. Iida, T. Sakamoto and H. Kawaura, *Appl. Phys. Lett.*, 2003, **83**, 1468.
22 W. D. Volkmuth and R. H. Austin, *Nature*, 1992, **358**, 600–602.
23 K. Inatomi, S. Izuo, S. Lee, H. Ohji and S. Shiono, *Microelectron. Eng.*, 2003, **70**, 13–18.
24 Y. C. Chan, Y. K. Lee and Y. Zohar, *J. Micromech. Microeng.*, 2006, **16**, 699–707.
25 O. Bakajin, T. A. J. Duke, J. Tegenfeldt, C. F. Chou, S. S. Chan, R. H. Austin and E. C. Cox, *Anal. Chem.*, 2001, **73**, 6053–6056.
26 S. Yi, K. S. Seo and Y. H. Cho, *Sens. Actuators, A*, 2005, **120**, 429–436.
27 Y. C. Chan, Y. Zohar and Y.-K. Lee, *Electrophoresis*, 2009, **30**, 3242.
28 R. Ogawa, H. Ogawa, A. Oki, S. Hashioka and Y. Horiike, *Thin Solid Films*, 2007, **515**, 5167–5171.
29 J. Han and H. G. Craighead, *Anal. Chem.*, 2002, **74**, 394–401.
30 T. Sano, N. Iguchi, K. Iida, T. Sakamoto, M. Baba and H. Kawaura, *Appl. Phys. Lett.*, 2003, **83**, 4438.
31 W. De Malsche, H. Eghbali, D. Clicq, J. Vangelooven, H. Gardeniers and G. Desmet, *Anal. Chem.*, 2007, **79**, 5915–5926.
32 H. Eghbali, S. Matthijs, V. Verdoold, H. Gardeniers, P. Cornelis and G. Desmet, *J. Chromatogr., A*, 2009, **1216**, 8603–8611.
33 B. He, N. Tait and F. Regnier, *Anal. Chem.*, 1998, **70**, 3790–3797.
34 B. He, J. Ji and F. E. Regnier, *J. Chromatogr., A*, 1999, **853**, 257–262.
35 B. E. Slentz, N. A. Penner and F. E. Regnier, *J. Chromatogr., A*, 2003, **984**, 97–107.
36 Z. He, Y. Li, Q. Zhang and H. Wang, *Appl. Catal., B*, 2009, **93**, 376–382.
37 G. Chen, G. T. McCandless, R. L. McCarley and S. A. Soper, *Lab Chip*, 2007, **7**, 1424–1427.
38 B. J. Hindson, D. M. Gutierrez, K. D. Ness, A. J. Makarewicz, T. R. Metz, U. S. Setlur, W. B. Benett, J. M. Loge, J. B. W. Colston, P. S. Francis, N. W. Barnett and J. M. Dzenitis, *Analyst*, 2008, **133**, 248–255.
39 T. Nissilä, L. Sainiemi, S. Franssila and R. Ketola, *Sens. Actuators, B*, 2009, **143**, 414–420.
40 G. K. Kiema, M. O. Jensen and M. J. Brett, *Chem. Mater.*, 2005, **17**, 4046–4048.
41 K. D. Harris, M. J. Brett, T. J. Smy and C. Backhouse, *J. Electrochem. Soc.*, 2000, **147**, 2002–2006.
42 M. M. Hawkeye and M. J. Brett, *J. Vac. Sci. Technol., A*, 2007, **25**, 1317–1335.
43 K. M. Krause, M. T. Taschuk, K. D. Harris, D. A. Rider, N. G. Wakefield, J. C. Sit, J. M. Buriak, M. Thommes and M. J. Brett, *Langmuir*, 2010, **26**, 4368.
44 K. Kaminska, T. Brown, G. Beydaghyan and K. Robbie, *Appl. Opt.*, 2003, **42**, 4212–4219.
45 A. K. Kar, P. Morrow, X. Tang, T. C. Parker, H. Li, J. Dai, M. Shima and G. Wang, *Nanotechnology*, 2007, **18**, 295702.
46 J. J. Steele, M. T. Taschuk and M. J. Brett, *IEEE Sens. J.*, 2008, **8**, 1422–1429.
47 I. Abdulhalim, A. Karabchevsky, C. Patzig, B. Rauschenbach, B. Fuhrmann, E. Eltzov, R. Marks, J. Xu, F. Zhang and A. Lakhtakia, *Appl. Phys. Lett.*, 2009, **94**, 063106.
48 S. Shanmukh, J. Driskell, Y. Zhao, R. Dluhy and R. A. Tripp, *Nano Lett.*, 2006, **6**, 2630–2636.
49 S. R. Jim, M. T. Taschuk, G. E. Morlock, L. W. Bezuidenhout, W. Schwack and M. J. Brett, *Anal. Chem.*, 2010, **82**, 5349–5356.
50 A. B. Jemere, L. W. Bezuidenhout, M. J. Brett and D. J. Harrison, *Rapid Commun. Mass Spectrom.*, 2010, **24**, 2305–2311.
51 S. W. Turner, A. M. Perez, A. Lopez and H. G. Craighead, *J. Vac. Sci. Technol., B*, 1998, **16**, 3835–3840.
52 D. S. Kim, H. U. Lee, N. H. Kim, K. Lee, D. Cho and T. H. Kwon, *Microelectron. Eng.*, 2007, **84**, 1532–1535.
53 K.-S. Yun and E. Yoon, *Lab Chip*, 2008, **8**, 245–250.
54 Y. Zeng, M. He and D. J. Harrison, *Angew. Chem.*, 2008, **120**, 6488–6491.
55 A. L. Elias, K. D. Harris, C. W. M. Bastiaansen, D. J. Broer and M. J. Brett, *J. Micromech. Microeng.*, 2005, **15**, 49–54.
56 N. Nazemifard, S. Bhattacharjee, J. H. Masliyah and D. J. Harrison, *Angew. Chem.*, 2010, **122**, 3398–3401.
57 Y.-P. Zhao and J.-G. Fan, *Appl. Phys. Lett.*, 2006, **88**, 103123.
58 J. K. Kwan and J. C. Sit, *Nanotechnology*, 2010, **21**, 295301.
59 J.-G. Fan, J.-X. Fu, A. Collins and Y.-P. Zhao, *Nanotechnology*, 2008, **19**, 045713.
60 J. N. Lee, C. Park and G. M. Whitesides, *Anal. Chem.*, 2003, **75**, 6544–6554.
61 A. L. Elias, K. D. Harris and M. J. Brett, *J. Microelectromech. Syst.*, 2004, **13**, 808–813.
62 K. M. Krause, M. Thommes and M. J. Brett, *Microporous Mesoporous Mater.*, 2011, DOI: 10.1016/j.micromeso.2011.02.023.
63 N. Nazemifard, L. Wang, W. Ye, S. Bhattacharjee, J. H. Masliyah and D. J. Harrison, *Lab Chip*, submitted.
64 N. Kaji, A. Oki, R. Ogawa, Y. Takamura, T. Nishimoto, H. Nakanishi, Y. Horiike, M. Tokeshi and Y. Baba, *Isr. J. Chem.*, 2007, **47**, 161–169.
65 D. Vick, T. Smy and M. J. Brett, *J. Mater. Res.*, 2002, **17**, 2904–2911.
66 C. Patzig, C. Khare, B. Fuhrmann and B. Rauschenbach, *Phys. Status Solidi B*, 2010, **247**, 1322–1334.
67 M. O. Jensen and M. J. Brett, *IEEE Trans. Nanotechnol.*, 2005, **4**, 269–277.

